

Supercurrents in Magnesium Diboride/Metal Composite Wire

M. J. Holcomb

*Novē Technologies, Inc.
3380 South Lapeer Road
Metamora, Michigan 48455 USA*

(main) 810-678-8014 (fax) 310-388-1370 (email) mholcomb@novewire.com

Abstract

We have fabricated a series of *ex situ* copper sheathed powder-in-tube MgB₂ wires with 20% by volume Ag, Pb, In, and Ga metal added to the MgB₂ powder. We find the transport critical current of these wires increases significantly with the addition of specific metals to the core filament. In particular, the critical current density (J_C) of the MgB₂/Ga(20%) wire is in excess of 5×10^4 A/cm² at 10K in self field, nearly 50 times that of the MgB₂/Ag(20%) wire. The temperature dependent J_C of all wires is well described as an ensemble of clean S/N/S junctions in which the relevant parameters are the average thickness of the *N* layer, the critical temperature of the *S* layer, and a scaling term related to J_C at zero temperature. Eliminating the differences in the filament microstructure as the primary cause of the enhanced J_C, we suggest that J_C is determined by the magnitude of the proximity effect induced superconductivity in the normal metal layer, which is known to be proportional to the electron-electron interaction in *N*. We present one-dimensional material specific calculations that support this, and zero-field cooled DC magnetic susceptibility data that confirm an increased number of well-connected superconducting grains exist in the composite wires that contain metal additions with large electron-electron interactions and long electron mean free paths.

PACS: 74.70.Ad, 74.60.Jg, 74.50.+r, 74.80.-g

Keywords: MgB₂; Metal powder addition, Proximity effect, Critical current density.

I. Introduction

The discovery of superconductivity near 40K in magnesium diboride (MgB_2) [1] sparked a worldwide effort to develop technically useful MgB_2 -based conductors for use in superconducting applications at temperatures less than 30K. Recent improvements in the current carrying properties of MgB_2 wire and tape in modest magnetic fields [2, 3], and the low materials cost of MgB_2 , suggest that these conductors may be economically competitive with technical NbTi and Nb_3Sn wire at 4.2K. Further, for superconducting applications in the 20K to 30K temperature range, which precludes the use of both NbTi and Nb_3Sn wire, MgB_2 wire and tape represent an inexpensive alternative to commercial high-temperature superconductor (HTS) tapes. With a significantly lower materials cost relative to HTS tape, the development of high critical current MgB_2 wire and tape may enable the economic adoption of superconducting devices such as transformers, motors, generators, and MRI magnets operating at temperatures above 20K in modest magnetic fields.

Similar to HTS ceramics [4], MgB_2 is mechanically brittle and not easily drawn into a fine wire. Unlike HTS ceramics, however, supercurrent flow in polycrystalline MgB_2 is not significantly impeded by the grain boundaries due to the relatively long coherence length of the material [5, 6] and the metallic nature of the grain boundaries [7]. These characteristics have allowed for the relatively rapid development of MgB_2 wire and tape

with critical current densities (J_C) in the range of 10^4 to 10^6 A/cm² at 4.2K in modest magnetic fields (< 4 Tesla) by a number of groups worldwide [8, 9, 10, 11, 12, 13, 14, 15, 16, 17, 18, 19, 20, 21, 22, 23, 24].

Flükiger has recently reviewed the development status of MgB₂ wires and tapes [25].

Although a number of methods have been investigated to fabricate MgB₂-based conductors, the most successful to date is the powder-in-tube (PIT) method. In general,

MgB₂ wire and tape fabrication is achieved using so-called *in situ* or *ex situ* PIT methodologies. In the *in situ* PIT method, stoichiometric amounts of magnesium and boron powder are well mixed and packed into a metal tube, which is sealed and drawn into wire. The wire is typically annealed between 600°C to 950°C with a variety of heating schedules to form a well-connected superconducting MgB₂ central filament.

Critical current densities of *in situ* MgB₂ PIT wires are limited by filament porosity, partially reacted precursor material, and deleterious reactions of Mg, B, or MgB₂ with the metal sheath material. A distinct advantage of the *in situ* PIT method is the ability to introduce nano-sized artificial pinning centers to the MgB₂ core filament [2], which has been shown to significantly increase the J_C of these conductors in applied magnetic fields.

In contrast, the *ex situ* PIT method of fabricating MgB₂ wire and tape is very similar to the *in situ* method except for the fact that MgB₂ powder is packed into the metal billet.

Although critical current densities in excess of 10^5 A/cm² at 4.2K in self-field [12] have

been reported on unsintered *ex situ* MgB₂ tape, a final high temperature anneal, which establishes a well-connected superconducting filament, generally leads to a significantly increased J_C in these conductors. A number of factors have been identified which affect the final J_C of *ex situ* MgB₂ conductors, these include the phase purity and morphology of the MgB₂ powder, the reactivity of MgB₂ with the metal sheath, and the final heat treatment schedule. Despite a number of factors which limit the J_C of *in situ* or *ex situ* MgB₂ wires and tapes, development has proceeded steadily and transport J_Cs in excess of 10⁵ A/cm² at 4.2K in self-field have been achieved in small coils made using multiple meter lengths of MgB₂ PIT wire and tape [13, 16, 26].

In addition to possessing high J_Cs in applied magnetic fields at temperatures less than 30K, technical MgB₂ wire and tape must also possess good thermal and mechanical stabilization. This depends critically on the metal sheath material used to encase the MgB₂ filaments. It is well known that high current NbTi and Nb₃Sn wire achieve stability by fabricating the wire with many thin superconducting filaments, which are embedded within a high purity stabilizing matrix [27] such as copper or aluminum. In order to fabricate stabilized multi-filamentary MgB₂ conductors, the sheath material must also possess sufficient ductility and strength to lend itself to common PIT wire and tape fabrication techniques, and must be relatively unreactive to Mg, B, or MgB₂ at the required annealing temperatures. A variety of sheath materials for MgB₂ wires and tapes

have been explored in the literature including Cu, Ag, Fe, Ni, Nb, Monel, and stainless steel [8-26]. Although copper is a very good, low cost stabilizing material, the tendency for Cu to form intermetallics with Mg at temperatures in excess of 650°C makes it less satisfactory as a sheath for MgB₂ [28, 29, 30].

The vast majority of high J_C MgB₂ wires and tapes in the literature are sheathed in either Fe or Ni. Although less reactive than Cu, these materials have also been found to react with Mg, B, or MgB₂ at temperatures in excess of 850°C forming Fe₂B [31] or Mg₂Ni [32], respectively. Further, the use of Fe, or Ni as sheath materials, with high electrical resistivities and low thermal conductivities with respect to high purity copper, results in conductors which tend to quench at transport currents well below the intrinsic I_C of the MgB₂ filament. This is implicit in the literature data on Fe- or Ni-sheathed MgB₂ wire and tape in that most high J_{CS} ($>10^4$ A/cm²) are obtained inductively, and many high transport I_Cs are obtained with short duty-cycle current pulses. Overall, the development of high I_C MgB₂ wire and tape with adequate thermal and mechanical stabilization remains a significant barrier to the adoption of these conductors in superconducting applications at temperature below 30K.

In principle, the fabrication of high I_C copper sheathed *ex situ* MgB₂ PIT wire is also feasible if it is possible to establish well-connected MgB₂ grains *without* employing high-temperature heat treatments. For example, increased I_{CS} in unsintered *ex situ* MgB₂ PIT

wire have been observed by a number of groups with the addition of a normal metal powder to the MgB_2 core filament [33, 34, 35, 36]. In particular, Tachikawa *et al.* [33, 34] reported a J_{C} enhancement of nearly a factor of five in MgB_2 PIT wire with the addition of 10% by volume indium to the core filament and employing a low temperature ($< 200^{\circ}\text{C}$) heat treatment. While this increase is much less than that realized through high temperature anneals of *in situ* or *ex situ* MgB_2 wire, it does suggest the use of normal metal additions to as a means of increasing the density of well-connected MgB_2 grains in the filament. It has been proposed that the increase of J_{C} in MgB_2 PIT wire with metal additions to the core filament may be due to an increase of the intra-filament thermal stability resulting from the addition of a metal with low electrical resistivity and high thermal conductivity [36], an improvement in the MgB_2 “grain linkage” presumably resulting from an increased Josephson current between the grains, or a proximity effect within the normal metal [34], an increased densification of the core filament, or a combination of all of these factors.

Here we report the systematic study of the effects of normal metal additions (Ag, In, Pb, and Ga) to *ex situ* copper sheathed MgB_2 PIT wire fabricated with no post deformation heat treatments. We find the core density and microstructure of the wires with 20% by volume Ag, In, and Pb to be nearly identical. However, the $I_{\text{C}}(10\text{K}$, self-field) of the wire with 20% by volume In metal added to the filament is over 30 times greater than that of the wire with 20% by volume Ag at 10K. We also find that, unlike the

wires with Ag, In, and Pb added to the filament, the filament of the MgB_2 PIT wire with 20% by volume Ga is inhomogeneous on the length scale of the filament diameter and displays significant alloying with the sheath at the Cu/filament interface. Despite this, we find that the I_C of the MgB_2 PIT wire with 20% by volume Ga is nearly 50 times greater than that of the MgB_2 PIT wire with 20% by volume Ag, and over 60 times greater than that of the MgB_2 PIT wire with no metal addition. We suggest that the primary reason for the significantly increased I_C of these wires is an increased MgB_2 grain connectivity due to the superconducting proximity effect in the normal metal, and not simply the result of increased filament density or intra-filament thermal stability.

This paper is divided into five sections. In section II we describe briefly the fabrication and characterization of all MgB_2 -based PIT wires reported in this study. In section III we describe the theoretical model used to interpret these data, and then discuss the implications of these results in section IV. In the Conclusions section, we summarize our results and discuss further this approach to the fabrication of high I_C *ex situ* MgB_2 conductors, with emphasis on the technical requirements necessary for superconducting device applications at temperatures less than 30K.

II. Experimental

A series of copper sheathed *ex situ* MgB_2 monofilament wires has been fabricated using standard techniques [4]. All wires were made with 20% by volume metal added to

the core filament. Previous studies indicate that the maximum J_C at 4.2K in self-field is obtained with approximately 15% to 35% by volume metal addition for both $\text{Nb}_3\text{Sn}/\text{Metal}$ [37] and $\text{MgB}_2/\text{Metal}$ [38] PIT wires using -325 mesh superconductor powders. These data and similar results obtained by Tachikawa *et al.* [34] suggested the selection of 20% by volume metal addition for all wires in this study.

The MgB_2 powder used to fabricate all samples was obtained from Alfa Aesar (-325 mesh, 99.9% metals basis). The as-received MgB_2 was sieved in an argon inert atmosphere box using a 450 mesh (32 μm) stainless steel sieve. Only the -450 mesh fraction of the MgB_2 was used in the fabrication of the wires in this study. In addition to a control MgB_2 PIT wire, four additional wires were fabricated using 20% by volume metal added to the MgB_2 powder [39]. The metal additions consisted of silver (0.5-1 μm , 99.9%, Alfa Aesar), indium (-325 mesh, 99.99%, Alfa Aesar), lead (-200 mesh, 99.9%, Alfa Aesar), and gallium (liquid, 99.999%, Alfa Aesar).

All $\text{MgB}_2/\text{Metal}$ (20% by volume), $\text{MgB}_2/\text{M}(20)$, composites were prepared using a Fritsch planetary mill housed in an inert atmosphere box under argon (< 1ppm O_2). The milling of the composites was designed to homogenize the component materials and not necessarily to reduce the MgB_2 particle size. The materials were milled at 500RPM for 2 hours in an 80ml stainless steel vial containing five 10mm diameter WC balls and one 25mm diameter WC ball. After planetary milling, the respective composite powders were each packed under argon into clean, 18cm long, alloy 110 copper billets (OD 9.53mm, ID

6.35mm), which were previously annealed at 650°C for 1 hour in an argon atmosphere.

After packing, the billet ends are sealed with soft copper plugs and Wood's metal before removal from the inert atmosphere. The sealed billets were drawn to 0.984mm diameter wire using a hydraulic draw bench and a 10% reduction schedule [40]. All billets were reduced to the final wire diameter with no intermediate heat treatments.

X-ray powder patterns of post-milled MgB₂ and MgB₂/M(20) composite powders were obtained on a Rigaku miniflex powder diffractometer using Cu K α radiation. These data indicate that there was no detectable degree of contamination from the milling media by XRD (~0.5% by volume sensitivity). However, trace amounts of Mg metal and oxides of magnesium and boron were detected by XRD. These are common contaminants in commercially available MgB₂.

Figure 1 shows polished transverse cross-sections and composite micrographs of the as-drawn wires. In general, all wires display good filament uniformity with an approximate filament diameter of 700 μ m. Figures 1(b) through (d) show the filament cross-section and micrograph of the MgB₂/Ag(20), MgB₂/In(20), and MgB₂/Pb(20) wires, respectively. These filaments consist of a distribution of MgB₂ particles, with a maximum diameter of approximately 10 μ m, in intimate contact with the added metal. The planetary milling process has significantly reduced the average domain size of the starting In and Pb powders (<44 μ m and <74 μ m, respectively), and in all three samples has resulted in a

nearly homogeneous distribution of material at the filament diameter length scale. The $\text{MgB}_2/\text{Ga}(20)$ wire cross-section, shown in Figure 1(e), is unique in that the distribution of Ga metal within the filament is not uniform. The light regions in the Figure represent domains of high Ga content. In addition, there is a region at the interface between the Cu sheath and the $\text{MgB}_2/\text{Ga}(20)$ filament in which there is significant alloying of the Cu and Ga. This is shown in Figure 2 where it is seen that there is an approximately $10\mu\text{m}$ wide interfacial region between the Cu and the filament core. Compositional analysis of this region indicates that it consists of approximately 63% atomic Ga. Figure 2 also shows a higher concentration of Ga metal within approximately $20\mu\text{m}$ of the sheath/filament interface. This increased concentration of Ga may result from the compressive forces experienced during the drawing of the wire, which force molten Ga out of the initially homogeneous mixture.

The starting billet filament fill factor % (i.e. the percentage of the total billet cross-section that is filament) for all samples is 44%. We find that this percentage is preserved during the wire drawing process for all samples [41], with a total measured variation in the filament fill factor % of approximately 5%. In contrast, we find that the filament packing fraction % (i.e. the percentage of actual mass of material in the filament to the theoretical limit) decreased from approximately 70 to 80% in the starting billet to approximately 60% for all samples when the billet was drawn into a wire [42]. Exceptions to this are the $\text{MgB}_2/\text{Pb}(20)$ wire which decreased from 77% in the billet to

73% in the as-drawn wire, and the MgB_2 PIT wire which decreased dramatically from 68% in the billet to only 33% of the theoretical limit in the as-drawn wire.

Transport critical current I_C measurements were determined using the $1\mu\text{V}/\text{cm}$ electric field criterion at temperatures ranging from 4.2K to 40K in self-field. Critical current densities J_C were calculated using the average measured cross-sectional area of the filament. If possible, n -values were calculated from the electric field versus current data at electric fields in excess of $1\mu\text{V}/\text{cm}$ and less than $10\mu\text{V}/\text{cm}$ [43, 44, 45]. Unless indicated otherwise, the superconducting transport properties of these wires, at temperatures greater than 4.2K in self-field, were determined using a hairpin probe design. One disadvantage associated with this measurement probe is that it is necessary to bend the wire over a forming mandrel prior to the measurement. The result is that all transport I_C measurements have been measured under approximately 2% bending strain, which results from bending a 0.984mm diameter wire over a 50mm diameter mandrel prior to mounting the sample on the probe [46]. For low transport currents (i.e. $< 10\text{A}$), we observe an approximately 20% reduction in I_C determined using the hairpin probe versus a straight sample I_C probe for all $\text{MgB}_2/\text{M}(20)$ wires in this study. However, we find a 2 to 3 time reduction in the I_C of the MgB_2 PIT wire when measured using the hairpin probe versus a straight sample I_C probe, indicating the inherently low strain tolerance of as-drawn *ex situ* MgB_2 PIT wire. The increase in strain tolerance of *ex situ*

MgB_2 PIT wires with normal metals added to the core filament has been observed previously [35].

Electric field versus DC transport current measurements for MgB_2 and $\text{MgB}_2/\text{M}(20)$ PIT wires at 10K in self-field are shown in Figure 3. The measured I_C , J_C , and n-value for these wires are listed in Table I. The MgB_2 PIT wire, with a J_C of 0.85 kA/cm^2 , is significantly lower than literature values which can be in excess of 100 kA/cm^2 at 10K. However, this J_C is not unreasonable given the as-drawn (i.e. unannealed) nature of the wire and the unusually low filament packing fraction %. While the addition of 20% by volume Ag to the filament does little to enhance the transport properties of the wire, the addition of Pb, In, or Ga metal to the MgB_2 filament results in a significant increase in I_C of the wire. In particular, the addition of 20% by volume Ga metal to the core filament results in a nearly 50 fold increase in the I_C of the wire at 10K. This is a remarkable result given that the $\text{MgB}_2/\text{Ga}(20)$ wire is the *least* homogeneous of all the wire samples. The $\text{MgB}_2/\text{Ag}(20)$, $\text{MgB}_2/\text{Pb}(20)$, and $\text{MgB}_2/\text{In}(20)$ wires possess nearly identical microstructures (Figure 1(b)-(d)), yet show dramatic increases in both I_C and n-value with the addition of Ag, Pb, and In, respectively.

The temperature dependent transport properties in self-field of MgB_2 and $\text{MgB}_2/\text{M}(20)$ PIT wires are shown in Figure 4. These data were collected from several 25cm sections of wire selected from a central 5m section of wire. Because the temperature of the measurement probe is not under active control, data from at least four

different wire sections at several different temperatures are plotted in the Figure. The low variance observed in the temperature dependence of the measured I_C in these 25cm wire sections indicates a high degree of filament uniformity over the central 5m of wire. Figure 4(a) shows the J_C and I_C of all wires fabricated in this work. From the Figure it is seen that the J_C of the $MgB_2/Ga(20)$ wire is approximately 50 times that of the $MgB_2/Ag(20)$ wire at temperatures up to approximately 25K. Figure 4(b) shows the n-value for all samples tested at temperatures greater than 10K. Again, the $MgB_2/Ga(20)$ shows the best performance with measured n-values in excess of 40 at 15K, and in excess of 20 at 20K in self-field. In general, the $MgB_2/M(20)$ series wires, all with approximately the same filament packing fraction %, display a clear trend of increasing I_C and n-value with the addition of 20% by volume Ag, Pb, In, and Ga, respectively.

III. Data Analysis

Our results indicate a clear enhancement in the current carrying properties of *ex situ* MgB_2 -based PIT wires with the addition certain normal metals to the MgB_2 filament. Other groups have also observed similar increases in the I_C of MgB_2 -based PIT wires and have suggested several possible reasons for such an enhancement [33, 34, 36]. These include an improvement in the MgB_2 “grain linkage” resulting from an increased Josephson current between the grains or a proximity effect within the normal metal, an

increased densification of the core filament, and an increase of the intra-filament thermal stability.

We analyze our results based on the schematic model of an ideal $\text{MgB}_2/\text{Metal}$ composite shown in Figure 5. In this model, MgB_2 particles are embedded within a ductile metal matrix in which individual MgB_2 particles are in contact with each other at well-defined contact points, and the ductile metal is localized within the interstitial regions of the composite. Although there are numerous direct $\text{MgB}_2/\text{MgB}_2$ contacts in the composite, the total area of these contacts is small relative to the $\text{MgB}_2/\text{Metal}/\text{MgB}_2$ contact area. Thus, we propose that the transport J_c of these composites may be described using the formalism developed to describe the J_c of conventional Superconductor/Normal/Superconductor (S/N/S) junctions. Essentially, we treat this ideal composite as a conglomeration of S/N/S junctions.

We assume that all S/N/S junctions in the $\text{MgB}_2/\text{M}(20)$ composite wires are in the clean limit ($l \gg \xi$), where l is inelastic mean free path of the electrons and ξ is the coherence length in N . In this limit, Hsiang and Finnemore [47] showed that the critical current density of a thick S/N/S junction in zero applied magnetic field approximately follows the relation,

$$J_c = J_0 (1 - T/T_c)^2 \exp(-K_N d), \quad (1)$$

where T_C is the superconducting critical temperature of S , d is the thickness of the normal metal layer N , J_0 is the maximum critical current density of the $S/N/S$ junction at zero temperature, and K_N^{-1} is the proximity effect decay length in N . In the limiting case where the electron-electron interactions in N are negligible, this decay length can be written as [48, 49],

$$K_N^{-1} = \hbar v_F / (2\pi k_B T) \quad (2)$$

where v_F is the Fermi velocity in N , and k_B is Boltzmann's constant. Equation (2) is a simplified result, which is obtained when the temperature T is much greater than the superconducting critical temperature of the normal metal T_{CN} . As pointed out by Deutscher and de Gennes [49], when T approaches T_{CN} in S/N junctions with non-zero electron-electron interactions in N , K_N^{-1} diverges and equation (2) underestimates the extent of the proximity effect in N . In this work, the majority of the J_C measurements have been obtained at temperatures well in excess of $3T_{CN}$ of the normal metal addition and thus, we neglect the divergence of K_N^{-1} as $T \rightarrow T_{CN}$ in the fitting of these J_C data.

Figure 6 shows the results of fitting the MgB_2 PIT and $MgB_2/M(20)$ J_C data to equation (1) using literature values for the Fermi velocities of the metals [50, 51]. The best fit parameters are tabulated in Table II, along with specific relevant parameters evaluated at 20K. The measured J_C of all wires in this study fit the model remarkably well using only three fitting parameters; d , T_C , and J_0 . Referring to Equation (1) it is seen that

the functional form of the critical current density in $S/N/S$ junctions is completely determined by the critical temperature of the superconductor, and the thickness and Fermi velocity of the normal metal. The J_0 term is simply a scaling factor.

The results of these model fits reveal certain characteristics of the supercurrent transport mechanism in these composites. In particular, the thickness of the normal metal layer d we interpret as the average distance between individual MgB_2 particles in the $MgB_2/M(20)$ composite filament, which carries the majority of the transport supercurrent. From Table II, it is seen that d is on the order of 1500\AA for all $MgB_2/M(20)$ samples. It is not surprising that this distance is on the order of the proximity effect decay length in N (e.g. K_N^{-1} at 20K in Table II), as the majority of the supercurrent in the composite likely flows through the large area $MgB_2/\text{Metal}/MgB_2$ contacts within K_N^{-1} of the S/N interfaces.

Consistent with our interpretation of the normal metal layer thickness d obtained from the model fits, is the very short inter-particle distance obtained from the fit of the MgB_2 PIT J_C data. In this case, an inter-particle distance of approximately 300\AA suggests that thin *metallic* regions between the MgB_2 grains limit the supercurrent in unannealed *ex situ* MgB_2 PIT wire. Annealing *ex situ* MgB_2 PIT wire increases the inter-grain contact area, relieves strain in the material, and reorders the surface layer of the individual grains. This effectively shrinks the thickness of the MgB_2/MgB_2 grain boundary contacts and establishes a high current S/S interface. Note that the inter-grain contact distance obtained

from the temperature dependent I_c of *ex situ* MgB_2 PIT wire, and the metallic nature of the contact, is consistent with the MgB_2 grain boundary studies of Samanta, *et al.* [7].

These model fits also reveal that the T_c for all wire samples is approximately 33K to 34K, which is considerably lower than the bulk T_c of commercial MgB_2 . We interpret this T_c as the critical temperature of the MgB_2 at the particle *surface* adjacent to the N metal, and not the bulk value. This is consistent with mechanical milling studies of MgB_2 which indicate that the T_c of this material is lowered by the surface disorder and strain produced during the milling process [52]. All composites in this study were prepared using a planetary milling procedure and thus the MgB_2 surface T_c is most likely lower than the bulk value.

As mentioned previously, the J_0 term in equation (1) represents the maximum J_c of an $S/N/S$ junction at zero temperature. In conventional $S/N/S$ junctions this term is typically less than 10^7 A/cm² in thin films [47, 53]. In our MgB_2 and $MgB_2/M(20)$ composite wires, however, J_0 spans nearly two orders of magnitude and includes the macroscopic composite structure of the total wire cross section as well as the microscopic limits related to the maximum zero temperature J_c of the N layer.

IV. Discussion

Although the transport properties of the MgB_2 and $MgB_2/M(20)$ PIT wires are well described by the $S/N/S$ model described in the previous section, there is a question as to

why there is a nearly 50 fold increase in the I_c of the $MgB_2/Ga(20)$ wire versus the $MgB_2/Ag(20)$ wire. In principle, there are only three parameters that may account for the extremely large differences in the J_c of these wires; J_0 , d , and T_c . The T_c values obtained from the fits to these data are all approximately the same, thus the $(1-T_R)^2$ term in equation (1) cannot contribute to the large observed increases in J_c . Table II lists the value of the $(1-T_R)^2$ term at 20K for all wire samples. Also, Table II lists the values of the $Exp(-K_N d)$ term in equation (1) at 20K, using the Fermi velocity and thickness of the N layer for all wire samples. Here, the shorter inter-particle distance of the $MgB_2/Ga(20)$ composite relative to the $MgB_2/Ag(20)$ composite accounts for a small increase in the J_c of the composite on the order of a factor of 2. The only remaining parameter that can account for the increased J_c of $MgB_2/M(20)$ is the J_0 term. This factor depends on the total surface area of the S/N contacts in the composite, which is related to the filament density, and the microscopic properties of the N layer which limit the supercurrent flow.

A. J_c Enhancement through Filament Densification

It is well known that critical current densities in granular superconducting wires and tapes may be increased by increasing the density of the superconducting filament. Critical currents increase with filament densification in PIT wire and tape from an increased contact area between adjacent superconductor grains in the filament. Filament porosity in MgB_2 PIT wire is generally minimized using sheath materials with high toughness (i.e.

Fe or Ni) [12], intermediate and final heat treatments, compressive wire deformation procedures, or flat rolling the wire to a tape geometry. The low filament packing % (33%) of the MgB_2 PIT wire relative to all $\text{MgB}_2/\text{M}(20)$ wires accounts for the dramatically lower transport J_C of this wire. The increase in I_C of the $\text{MgB}_2/\text{M}(20)$ wires with Ag, Pb, In, and Ga, however, is not as easily assigned to a filament densification model because the filament packing fraction % of these wires is approximately 60%, with the exception of Pb at 73%. The lack of a correlation between filament density and I_C in $\text{MgB}_2/\text{M}(20)$ wires eliminates a simple filament densification model as an explanation for the increase in supercurrent transport of these wires.

Another possible reason for the enhanced I_C of $\text{MgB}_2/\text{M}(20)$ wires may be because of the relative hardness of the added metals. In our $S/N/S$ composite model, I_C will increase with increased S/N contact area. The most dramatic increases will occur with increased S/N contact areas that possess N layer widths on the order of K_N^{-1} . The hardness of a material is its resistance to a localized plastic deformation. In the fabrication of $\text{MgB}_2/\text{M}(20)$ PIT wire, the forces which deform the billet during the drawing process will cause the hard, brittle MgB_2 particles to deform the softer metal particles. This process forces the softer metal into the interstitial regions of the MgB_2 particle network in the filament [34], and may significantly increase the overall S/N contact area. The Brinell hardness of In, Ag and Pb is 8.83, 24.5, and 38.3, respectively [54]. Thus, although it is

difficult to quantify the increase in S/N surface area in the $\text{MgB}_2/\text{M}(20)$ composite, we would expect to see an increase in I_c in with the softer metals. The fact that the $\text{MgB}_2/\text{Pb}(20)$ wire possesses an I_c nearly 20 times that of the $\text{MgB}_2/\text{Ag}(20)$ wire is inconsistent with this model. However, the very high I_c of the $\text{MgB}_2/\text{Ga}(20)$ wire may in part be the result of the increased S/N contacts in the filament, as the Ga is clearly in the liquid state during the wire deformation process.

B. J_c Enhancement through the Superconducting Proximity Effect

It appears likely that slight differences in the $\text{MgB}_2/\text{M}(20)$ composite morphology may account for changes in J_c on the order of a factor of two, yet this increase remains well below the observed enhancement of the transport properties of $\text{MgB}_2/\text{M}(20)$ wires. We propose that the dramatically increased J_c in these wires may be due to the unique properties of the specific metal addition that is in intimate contact with the superconducting MgB_2 particles in the filament.

It is well known that when a superconductor is placed in contact with a normal metal, the Cooper pair amplitudes in the superconductor do not vanish abruptly at the S/N interface, but extend a significant distance into N . This phenomenon, characterized by the induction of superconducting properties in the otherwise normal metal within K_N^{-1} of the S/N interface, is known as the superconducting proximity effect [49, 55, 56, 57, 58]. Near the S/N interface, the normal metal exhibits superconducting properties such as a

reduction in the electronic density of states at the Fermi surface [59, 60, 61], and a significant Meissner effect [62, 63, 64, 65, 66, 67, 68]. In addition, S/N/S junctions are known to support supercurrents over distances much greater than K_N^{-1} at temperatures below T_c of the S layer [69, 47, 53].

Here we suggest that the observed increase in J_c of $MgB_2/M(20)$ PIT wires results from the magnitude of the proximity effect induced superconducting gap Δ in N , which is specific to each metal addition. In this case, the $S/N/S$ model junction discussed in Section III becomes an $S/S'/S$ junction where the S' layer is weakly superconducting [70] and J_0 is limited by the magnitude of the minimum Δ in the S' layer. Though a detailed calculation of the magnitude of Δ in $MgB_2/M(20)$ composites is an intractable problem, a reasonable first approximation may be obtained by solving for Δ in one-dimensional MgB_2 /Metal model junctions.

Extending the work of de Gennes [48, 70], McMillan showed that the magnitude of Δ in N is a function of both the Cooper pair amplitude and the magnitude of the electron-electron interaction in N [56]. With a first approximation that $\Delta(x)$ is constant in S and zero in N , the spatial dependence of the superconducting gap $\Delta(x)$ in S/N junctions is determined self-consistently from,

$$\Delta(x) = \lambda^*(x)F(x) , \quad (3)$$

with [71],

$$\lambda^* = (\lambda - \mu^*)/(1 + \lambda) , \quad (4)$$

where $F(x)$ is the Cooper pair amplitude, λ is the electron-phonon coupling constant [72] and μ^* is the magnitude of the screened Coulomb repulsion [73]. This general method of solving for $\Delta(x)$ in S/N junctions has been extended recently to include junctions with different Fermi velocities and electron mean free paths [58]. In our work, we use numerical methods developed in the study of proximity effects in $S/N/N'$ junctions to calculate the magnitude of $\Delta(x)$ in model MgB_2 /Metal junctions at finite temperature. We also include the effects of finite electron mean free paths and differing Fermi velocities in the S and N layers [74].

The Cooper pair amplitude $F(x)$, normalized to its value deep within the bulk superconductor F_{Bulk} , for one dimensional MgB_2 /Metal junctions is shown in Figure 7(a). These data are calculated at 20K using the parameters listed in Table III, the v_F of MgB_2 listed in Table II, and an average $\Delta \sim 6.7$ meV at 20K for MgB_2 [75]. In general, $F(x)$ decreases with increasing distance from the S/N interface and this decrease is exponential with x for distances $\gg K_N^{-1}$ [49]. These calculations show that the Cooper pair amplitude in S/N junctions is severely attenuated by short electron mean free paths in the N layer [76]. In the Figure, it is seen that $F(x)$ extends several thousand Å into the N layer in the MgB_2 /Ag and MgB_2 /Ga model junctions because of the very long mean free paths of the electrons in Ag and Ga at 20K. In contrast, the high resistivity Pb layer in the MgB_2 /Pb

model junction has a much shorter mean free path, and thus the Cooper pairs do not extend as deeply into N .

Using the calculated Cooper pair amplitudes and the electron-electron coupling specific to each normal metal, the spatial dependence of the induced superconducting gap in N is obtained using equation (3). These data are shown in Figure 8(b), where it is clearly seen that $\Delta(x)$ in N scales linearly with λ^* . Normal metals with very low λ^* values, do not exhibit strong induced superconductivity even though there may be a large Cooper pair amplitude in N . Here we make a distinction between a large amplitude of correlated electron pairs in N , and a large Δ . The MgB_2/Ag model junction in Figure 7 shows this distinction clearly, where it is seen that even though $F(x)$ is very large in the Ag layer, the extremely low λ^* value specific to Ag metal results in a very small induced Δ . On the other hand, the MgB_2/Ga model junction has both a large Cooper pair amplitude, and a large λ^* in N . Thus, the Ga layer in the MgB_2/Ga model junction displays a large induced Δ .

From these model calculations, it is evident that there is a correlation between the physical properties of the N layer material and the magnitude of the induced Δ in N , which we propose is responsible for the enhanced J_C observed in $\text{MgB}_2/\text{M}(20)$ PIT wires. In Figure 8 we plot the measured J_C of each $\text{MgB}_2/\text{M}(20)$ wire at 20K vs. the magnitude of the induced Δ from Figure 7(b) at 500Å. We approximate the N layer thickness in

these three dimensional composites with a value of approximately 500Å in the one dimensional model, but also choose this value as it results in a very good correlation to these experimental data. This correlation is perhaps better than we should expect to obtain given the numerous simplifications of our model, yet we believe it provides strong evidence that the J_c of $MgB_2/M(20)$ composite wires is largely determined by a proximity effect induced Δ in the normal metal component of the composite.

Critical supporting evidence of the existence of a proximity effect limited J_c in $MgB_2/M(20)$ composite wires can be obtained from zero-field cooled (ZFC) DC magnetic susceptibility measurements. We follow the development of Thompson, *et al.* [77] where “non-ideal” granular superconductors were studied with DC magnetic methods. In granular superconductors, the intra-grain critical currents may be well in excess of the inter-grain critical currents. This is the case for example, in the HTS ceramics where weak link contacts at the grain boundaries are known to severely reduce the transport I_c of HTS PIT tape [78]. The magnitude and temperature dependence of the intra- and inter-grain I_c of granular superconductors may be determined using ZFC DC magnetic susceptibility measurements.

Figure 10 shows the ZFC DC magnetic susceptibility of all $MgB_2/M(20)$ composite wire in this study. These measurements were made on a Quantum Design SQUID magnetometer in an applied magnetic field of 10Oe. These data were obtained on 0.984mm diameter $MgB_2/M(20)$ wire samples approximately 5mm in length using the

measured filament packing fraction %, and are plotted as the volume susceptibility (emu/cm³). Thus, a direct comparison can be made between the as-measured susceptibility without including the geometric demagnetization factor for a cylinder [77]. As seen in Figure 9, the *onset* of a diamagnetic susceptibility in all samples occurs near 38K, and there is an increasing diamagnetic response of the MgB₂/M(20) composites with increasing λ^* and l of the N layer. In particular, as the MgB₂/Ga(20) sample is warmed in an applied magnetic field, the diamagnetic susceptibility decreases slightly up to approximately 20K, then exhibits an abrupt loss of diamagnetism near 30K. This is in contrast to the MgB₂/Ag(20) composite in which the relatively small diamagnetic response shows no distinct transition with increasing temperature. The MgB₂/Pb(20) and MgB₂/In(20) composites, however, display a sudden loss of diamagnetism with warming at approximately 15K and 20K, respectively. We associate the sudden loss of diamagnetism in the MgB₂/Pb(20), MgB₂/In(20), and MgB₂/Ga(20) composite wires with the temperature at which the induced surface currents exceed the inter-grain I_C . In general, these data show there is a significant *increase* in the volume of *well-connected* (i.e. superconducting) contacts in the MgB₂/M(20) composites with high λ^* normal metal additions with long electron mean free paths. This is a clear indication of the existence of a substantial proximity effect in these composite materials.

Conclusions

We have fabricated a series of *ex situ* copper stabilized MgB_2 PIT wires with different normal metals added to the core filament. We find that the transport critical current of these wires increases significantly with the addition of metals that possess both large electron-electron interactions and long electron mean free paths, and not due to the filament morphology. In particular, the temperature dependence and magnitude of the transport critical currents of $\text{MgB}_2/\text{M}(20)$ wires is well described as an ensemble of $S/\text{N}/S$ junctions in which the supercurrent is carried primarily by $\text{MgB}_2/\text{Metal}/\text{MgB}_2$ contacts with metal layer widths less than the de Gennes proximity effect decay length, K_N^{-1} . One-dimensional calculations of the magnitude of the proximity effect superconducting gap in $\text{MgB}_2/\text{Metal}$ model junctions support this, and ZFC DC magnetization data clearly indicate an increased number of well-connected superconducting contacts in the $\text{MgB}_2/\text{M}(20)$ composites which contain high λ^* metals with long l . These results provide strong evidence that the supercurrent in $\text{MgB}_2/\text{M}(20)$ composite wires is determined by inter-granular $S/\text{N}/S$ critical currents, which are in effect determined by the magnitude of the proximity effect induced superconducting gap within the N layer.

The driving force for this work is to develop a means to establish superconducting inter-grain contacts in *ex situ* MgB_2 PIT wire without the use of heat. This would not only allow for the use of low cost copper as a stabilizing matrix for these conductors, but in

principle should lower the fabrication costs with the elimination of a high temperature batch anneal. Further, the use of metal additions in these conductors has certain advantages, some of which have been documented in the literature and confirmed here. In particular, we have observed a significant increase in the strain tolerance of these wires as compared to *ex situ* MgB₂ PIT wire with no added metal. Also, the metal addition allows for the possibility of enhanced intra-filament stability due to the relatively high thermal conductivity of the added metal. This may be of particular importance in these conductors as it may be difficult to achieve the 1-5 μ m filament diameter typical of fully stabilized multifilamentary superconducting wire because of the relatively large MgB₂ particle size. Another advantage of this approach is that it allows for the addition of artificial pinning centers to the *normal metal layer* at relatively low temperatures. This may significantly improve the transport properties of MgB₂/Metal composite wires in applied magnetic fields.

Technical MgB₂ conductors, in addition to being low cost, must have high transport currents in modest magnetic fields. In general, superconducting applications such as transformers, motors, and generators require critical currents of at least 100A in approximately 1 to 2 Tesla at the operating temperature of the device. We have limited data on the transport properties of these conductors in applied magnetic fields. Figure 10(a) shows the transport critical current of MgB₂/Ga(20) wire at 4.2K in applied magnetic fields up to 6T [79]. The J_C of this wire decreases exponentially with increasing

magnetic field as anticipated from the behavior of S/N/S junctions in applied magnetic fields [47]. The n-value of MgB₂/Ga(20) wire as a function of applied magnetic field is shown in Figure 10(b), where it is seen to be in excess of 20 at 2T at 4.2K. Assuming a similar magnetic field response at 20K, we estimate that the MgB₂/Ga(20) wire will have a transport J_C in excess of 5×10^3 A/cm² in 1T magnetic field.

The measured transport critical currents in MgB₂/M(20) wires are less than what is required at present for practical superconducting devices, however, there is considerable room for improvement in these wires. Generally, I_C optimization based on the composite packing density, MgB₂/Metal volume %, MgB₂ particle size, and conductor geometry are relatively simple engineering improvements to these conductors. Other improvements can be achieved using additional characterization/fabrication methods. In particular, we find the MgB₂/Ga(20) wire has a relatively inhomogeneous cross-section, yet it possesses the highest transport current. This suggests there are regions within the wire that have *very* high critical currents. Magneto-optical studies performed on these conductors should help to elucidate where the supercurrent is flowing in this inhomogeneous composite. These results, in turn, should lead to significant improvements in the I_C of these conductors. Also, the insertion of thin barrier layers, similar to those used in the copper stabilized *in situ* MgB₂ multifilamentary wire fabricated by Sumption *et al.* [17], will significantly reduce the alloy formation at the copper/filament interface in MgB₂/Ga(20) wire and may

also lead to improved transport currents. In addition, the relatively low T_c at the MgB_2 particle surface is also limiting the supercurrent in these composites. A low-temperature post-mill anneal of the composite before packing into the billet may minimize this effect. Finally, because the superconducting proximity effect is known to be severely attenuated by the presence of insulating contaminants at the S/N interface, high quality MgB_2 powder is essential for the fabrication of high current $\text{MgB}_2/\text{Metal}$ PIT wire. Thus, significant improvements in the transport properties of $\text{MgB}_2/\text{Metal}$ PIT wire are expected with the use of high quality, high T_c MgB_2 powder.

Acknowledgements

The author would like to thank Dr. David A. Tyvoll, Professor William A. Little, Professor James P. Collman, and Dr. Todd Eberspacher for many valuable discussions, technical assistance, and comments. In addition, the author gratefully acknowledges Dr. Ken A. Marken (Oxford Superconductor Technology) for providing transport data as a function of applied magnetic field, Dr. Reza Loloei (Michigan State University, Center for Fundamental Materials Research) for valuable assistance in obtaining the DC susceptibility data, and Mike Tomsic (HyperTech Research), Dr. M.D Sumption and Dr. E.W. Collings (Ohio State University, Laboratory for Applied Superconductivity and Magnetism) for many useful discussions regarding superconducting wire. Partial

financial support provided by the California Energy Commission's Public Interest Energy Research group's Energy Innovations Small Grant Program.

References

- [1] J. Nagamatsu, N. Nakagawa, T. Muranaka, Y. Zenitani, and J. Akimitsu, *Nature* **410** (2001) 63.
- [2] X.L. Wang, Q.W. Yao, J. Horvat, M.J. Qin, and S.X. Dou, *Supercond. Sci. Technol.* **17** (2004) L21.
- [3] H. Kumakura, H. Kitaguchi, A. Matsumoto, and H. Hatakeyama, *Appl. Phys. Lett.* **84**, 3669 (2004).
- [4] T. P. Sheahen and A.M. Wolsky, in *Introduction to High Temperature Superconductivity*, Ch. 16, p. 317, (Plenum Press, New York) 1994.
- [5] D.C. Larbalestier, L.D. Cooley, M.O. Rikel, A.A. Polyanskii, J. Jiang, S. Patnaik, X.Y. Cal, D.M. Feldmann, A. Gurevich, A.A. Squitierl, M.T. Naus, C.B. Eom, E.E. Hellstrom, R.J. Cava, K.A. Regan, N. Rogado, M.A. Hayward, T. He, J.S. Slusky, P. Khalfah, K. Inumaru, and M. Haas., *Nature* **410**, 186 (2001).
- [6] D.K. Finnemore, J.E. Ostenson, S.L. Bud'ko, G. Lapertot, and P.C. Canfield, *Phys. Rev. Lett.* **86**, 2420 (2001)
- [7] S.B. Samanta, H. Narayan, A. Gupta, A.V. Narlikar, T. Muranaka, and J. Akimitsu, *Phys. Rev. B* **65**, 092510-1 (2002).
- [8] S. Soltanian, X.L. Wang, I. Kusevic, E. Babic, A.H. Li, M.J. Qin, J. Horvat, H.K. Liu, E. Lee, E.W. Collings, M.D. Sumption, and S.X. Dou, *Physica C* **361**, 84 (2001).
- [9] X.L. Wang, S. Soltanian, J. Horvat, A.H. Liu, M.J. Qin, H.K. Liu and S.X. Dou, *Physica C* **361**, 149 (2001).

- [10] M.D. Sumption, X. Peng, E. Lee, M. Tomsic, and E.W. Collings, cond-mat/0102441
- [11] S. Jin, H. Mavoori, C. Bower, and R.B. van Dover, *Nature* **411**, 563 (2001).
- [12] G. Grasso, A. Malagoli, C. Ferdeghini, S. Roncallo, V. Braccini, and A.S. Siri, *Appl. Phys. Lett.* **79**, 230 (2001).
- [13] T. Machi, S. Shimura, N. Koshizuka, and M. Murakami, *Physica C* 392-396, 1039 (2003).
- [14] B.Q. Fu, Y. Feng, G. Yan, C.F. Liu, L. Zhou, L.Z. Cao, K.Q. Ruan, and X.G. Li, *Physica C* 392-396, 1035 (2003).
- [15] R. Flükiger, P. Lezza, C. Beneduce, N. Musolino, and H.L. Suo, *Supercond. Sci. Technol.* **16** (2003) 264.
- [16] G. Grasso, A. Malagoli, M. Modica, A. Tumino, C. Ferdeghini, A.S. Siri, C. Vignola, L. Martini, V. Previtali, and G. Volpini, *Supercond. Sci. Technol.* **16** (2003) 271.
- [17] M.D. Sumption, M. Bhatia, X. Wu, M. Rindfleisch, M. Tomsic, and E.W. Collings, cond-mat/0409280.
- [18] W. Goldacker, S.I. Schlachter, B. Liu, B. Obst, and E. Klimenko, *Physica C* 401, 80 (2004).
- [19] P. Lezza, V. Abächerli, N. Clayton, C. Senatore, D. Uglietti, H.L. Suo, and R. Flükiger, *Physica C* 401, 305 (2004).
- [20] H. Fang, Y.Y. Xue, Y.X. Zhou, A. Baikalov, and K. Salama, *Supercond. Sci. Technol.* **17** (2004) L27.
- [21] H. Kitaguchi, A. Matsumoto, H. Hatakeyama, and H. Kumakura, *Supercond. Sci. Technol.* **17** (2004) S486.
- [22] W. Goldacker, S.I. Schlachter, B. Obst, B. Liu, J. Reiner, and S. Zimmer, *Supercond. Sci. Technol.* **17** (2004) S363.

[23] P. Kovác, I. Husek, T. Melisek, J.C. Grivel, W. Pachla, V. Strbík, R. Diduszko, J. Homeyer, and N.H. Andersen, *Supercond. Sci. Technol.* **17** (2004) L41.

[24] O. Perner, J. Eckert, W. Häßler, C. Fischer, K-H Müller, G. Fuchs, B. Holzapfel, and L. Schultz, *Supercond. Sci. Technol.* **17** (2004) 1148.

[25] R. Flükiger, H.L. Suo, N. Musolino, C. Beneduce, P. Toulemonde, and P. Lezza, *Physica C* 385, 286 (2003).

[26] S. Soltanian, J. Horvat, X.L. Wang, M. Tomsic, and S.X. Dou, *Supercond. Sci. Technol.* **16** (2003) L4-L6.

[27] F.M. Asner, in *High Field Superconducting Magnets*, Ch. 3, Clarendon Press, (1999).

[28] S. Zhou, A.V. Pan, M. Ionescu, H. Liu, and S. Dou, *Supercond. Sci. Technol.* **15** (2002) 236-240.

[29] B.A. Glowacki, M. Majoros, M. Vickers, M. Eisterer, S. Toenies, H.W. Weber, M. Fukotomi, K. Komori, and K. Togano, *Supercond. Sci. Technol.* **16** (2003) 297-305.

[30] E. Martínez, L.A. Angurel, and R. Navarro, *Supercond. Sci. Technol.* **15** (2003) 1043-1047.

[31] C.R.M. Grovenor, L. Goodsir, C.J. Salter, P. Kovac, and I. Husek, **17** (2004) 479-484.

[32] H.L. Suo, C. Beneduce, M. Dhalle, N. Musolino, J.E. Genoud, and R. Flükiger, *Appl. Phys. Lett.* **79**, 3116 (2001).

[33] K. Tachikawa, Y. Yamada, O. Suzuki, M. Enomoto, and M. Aodai, *Physica C* 382, 108 (2002).

[34] K. Tachikawa, Y. Yamada, M. Enomoto, M. Aodai, and H. Kumakura, *Physica C* 392-396, 1030 (2003).

[35] K. Katagiri, A. Iwamoto, Y. Shoji, K. Tachikawa, Y. Yamada, K. Watanabe, and T. Mito, *Physica C* 397, 95 (2003).

[36] P. Kovác, I. Husek, T. Melisek, C. R. M. Grovenor, S. Haigh, and H. Jones, *Supercond. Sci. Technol.* **17** (2004) 1225.

[37] M.J. Holcomb, T.A. Eberspacher, J.P. Collman, and W.A. Little (unpublished, Stanford University, 1998).

[38] D.A. Tyvoll, A.E. Lui, P.G. Wheelon and M.J. Holcomb (unpublished, Nové Technologies, 2001)

[39] In this study we report data obtained on five carefully prepared monofilamentary wire samples fabricated using identical methods. Since 2001, we have measured similar transport properties on well over a hundred MgB₂/Metal composite wires fabricated with a variety of metal additions. Although prepared by different methods, transport data obtained on all MgB₂/Metal composite wires are consistent with the results presented here.

[40] All wires in this study were drawn by HyperTech Research, Inc., Columbus, OH.

[41] Wire fill factor %: MgB₂ PIT = 42%, MgB₂/Ag(20) = 45%, MgB₂/In(20) = 43%, MgB₂/Pb(20) = 47%, MgB₂/Ga(20) = 44%.

[42] Filament packing %: MgB₂ PIT = 68%(billet) 33%(wire), MgB₂/Ag(20) = 68%(billet) 61%(wire), MgB₂/In(20) = 79%(billet) 60%(wire), MgB₂/Pb(20) = 77%(billet) 73%(wire), MgB₂/Ga(20) = 81%(billet) 63%(wire). In general, lower melting point metals were found to pack in the billet at a slightly higher packing fraction %.

[43] L.F. Goodrich and F.R. Fickett, *Cryogenics* **22**, (1982) 225-41.

[44] L.F. Goodrich and A.N. Srivastava, *Cryogenics* **35**, (1995) S19-S23.

[45] B. Seeber, p. 307 in *Handbook of Applied Superconductivity, Vol. 1*, Institute of Physics Publishing (1998).

[46] Bending strain is defined as the ratio of the diameter of the wire to the bending diameter.

[47] T.Y. Hsiang and D.K. Finnemore, *Phys. Rev.* **B22**, 154 (1980).

[48] P.G. de Gennes, *Rev. Mod. Phys.* **36**, 225 (1964)

[49] G. Deutscher and P.G. de Gennes in *Superconductivity*, Vol. 2, p. 1005, ed. R.D. Parks, Dekker, New York (1969).

[50] N.W. Ashcroft and N.D. Mermin in *Solid State Physics*, p. 38, W.B. Saunders Company (1976).

[51] S.V. Shulga, S.L. Drechsler, H. Eschrig, H. Rosner, and W. Pickett, cond-mat/0103154.

[52] Y.D. Gao, J. Ding, G.V.S. Rao, B.V.R. Chowdari, W.X. Sun, and Z.X. Shen, *Phys. Stat. Sol. (a)* **191**, No. 2, 548-554 (2002).

[53] Y.K. Kwong, K. Lin, M.S. Isaacson, and J.M. Parpia, *Phys. Rev. Lett.* **65**, 2905 (1990).

[54] Brinell hardness values from www.webelements.com

[55] N.R. Werthamer, *Phys. Rev.* **132**, 2440 (1963).

[56] W.L. McMillan, *Phys. Rev.* **175**, 559 (1968).

[57] G.B. Arnold, *Phys. Rev.* **B18**, 1076 (1978).

[58] Y. Tanaka and M. Tsukada, *Phys. Rev.* **B37**, 5095 (1988); *Phys. Rev.* **B47**, 287 (1993).

[59] S. Guéron, H. Pothier, N.O. Birge, D. Esteve, and M.H. Devoret, *Phys. Rev. Lett.* **77**, 3025 (1996).

[60] N. Moussy, H. Courtois, and B. Pannetier, cond-mat/0106299.

[61] A.K. Gupta, L. Crétinon, N. Moussy, B. Pannetier, and H. Courtois, *Phys. Rev.* **B69**, 104514 (2004).

[62] Y. Oda and H. Nagano, *Solid State Commun.* **35**, 631 (1980).

[63] Th. Bergmann, H. Kuhl, B. Schröder, M. Jutzler, and F. Pobell, *J. Low Temp. Phys.* **66**, 209 (1987).

[64] A.C. Mota, P. Visani, and A. Pollini, *J. Low Temp. Phys.* **76**, 465 (1989).

[65] H. Toyoda, A. Sumiyama, Y. Oda, and K. Asayama, *J. Phys. Soc. Japan* **62**, 672 (1993).

[66] W. Belzig, C. Bruder, and G. Schön, *Phys. Rev.* **B53**, 5727 (1996).

[67] F.B. Müller-Allinger, A.C. Mota, and W. Belzig, cond-mat/98090.

[68] D. Katayama, A. Sumiyama, and Y. Oda, , *Phys. Rev.* **B68**, 132502 (2003).

[69] J. Clarke, *Proc. Roy. Soc. London* **A308**, 447 (1969).

[70] P.G. de Gennes, in *Superconductivity of Metals and Alloys*, p. 155, Westview Press (1999).

[71] λ^* is equivalent to the electron pairing parameter $N(0)V$ in BCS theory.

[72] W.L. McMillan and J.M. Rowell, in *Superconductivity*, Vol. 1, p. 561, ed. R.D. Parks, Dekker, New York (1969).

[73] P. Morel and P.W. Anderson, *Phys. Rev.* **125**, 1263 (1962).

[74] A. Gama Goicochea, Ph.D. Thesis, Stanford University (1998).

[75] We set $2\Delta_0/k_B T_C = 4.0$ for these model calculations and assume an average $\Delta_0 = 7$ meV for MgB_2 . In this model, T_C is approximately 40K.

[76] N.W. Ashcroft and N.D. Mermin in *Solid State Physics*, p. 52, W.B. Saunders Company (1976).

[77] J.R. Thompson, D.K. Christen, H.R. Kerchner, L.A. Boatner, B.C. Sales, B.C. Chakoumakos, H. Hsu, J. Brynestad, D.M. Kroeger, R.K. Williams, Y.R. Sun, Y.C. Kim, J.G. Ossandon, A.P. Malozemoff, L. Civale, A.D. Marwick, T.K. Worthington, L.

Krusin-Elbaum, and F. Holtzberg, in *Magnetic Susceptibility of Superconductors and Other Spin Systems*, ed. R.A. Hein *et al.*, Plenum Press (1991).

[78] T. P. Sheahen, in *Introduction to High Temperature Superconductivity*, Ch. 13, p. 243, (Plenum Press, New York) 1994.

[79] Data provided by Dr. K.A. Marken, Oxford Superconducting Technology, Carteret, NJ.

Figure Captions

Figure 1. SEM microstructures of MgB_2 and $\text{MgB}_2/\text{M}(20)$ wires. The left column shows the transverse cross-section of the as-drawn wires and the right column shows the average microstructure of the core filament.

Figure 2. SEM micrograph of the Copper/[$\text{MgB}_2/\text{Ga}(20)$] interface. The $\sim 10\mu\text{m}$ wide region at the interface consists of a CuGa alloy containing approximately 63% atomic Ga.

Figure 3. Electric field versus current measurements for MgB_2 and $\text{MgB}_2/\text{M}(20)$ PIT wires at 10K in self field. The slight negative bias of these data at high transport currents ($>100\text{A}$) results from an inductive pick-up in the voltage leads. The dashed line in the Figure indicates the $1\mu\text{V}/\text{cm}$ electric field criterion at which I_C is determined. Note the $\text{MgB}_2/\text{Ga}(20)$ PIT wire tends to quench at transport currents in excess of 150A.

Figure 4. Temperature dependent transport properties of MgB_2 and $\text{MgB}_2/\text{M}(20)$ PIT wires in self-field. (a) The critical current density (J_C) and critical current (I_C) of all wires as determined using the $1\mu\text{V}/\text{cm}$ electric field criterion. (b) The n -value of all wires as determined from the electric field versus current data from $1\mu\text{V}/\text{cm}$ to $10\mu\text{V}/\text{cm}$.

Figure 5. Schematic diagram of an ideal $\text{MgB}_2/\text{Metal}$ composite used to interpret the transport properties of $\text{MgB}_2/\text{M}(20)$ PIT wire. In this model, the large $\text{MgB}_2/\text{Metal}$ contact area determines the transport properties of the composite. Thus, these composites are essentially a conglomeration of S/N/S junctions.

Figure 6. Temperature dependent transport properties of MgB_2 and $\text{MgB}_2/\text{M}(20)$ PIT wires in self-field (symbols) and the best fit of these data using a $S/N/S$ model in the clean

limit (solid lines). From the Figure it is easily seen that there is very good agreement between experiment and theory based on a simple *S/N/S* model describing the transport properties of these wires.

Figure 7. Proximity effect calculations for one-dimensional $\text{MgB}_2/\text{Metal}$ junctions at 20K.

(a) Cooper pair amplitude $F(x)$ as a function of distance for each model junction normalized to the amplitude of the Cooper pairs deep within the bulk superconducting MgB_2 . (b) Superconducting gap $\Delta(x)$ as a function of distance for each model junction. The magnitude of $\Delta(x)$ in N is proportional to the magnitude of the electron-electron interaction λ^* in N .

Figure 8. Experimental transport properties of $\text{MgB}_2/\text{M}(20)$ PIT wires versus the calculated magnitude of a proximity induced superconducting gap at 500Å in the normal metal layer. This correlation provides strong evidence that the transport properties of $\text{MgB}_2/\text{M}(20)$ PIT wires are largely determined by the magnitude of the proximity effect in the N layer, which is specific to each metal addition.

Figure 9. Zero-field cooled DC magnetic susceptibility of $\text{MgB}_2/\text{M}(20)$ PIT wire. These data show a clear increase in the well-connected diamagnetic volume of superconducting material in these composites, which contain metals with large electron-electron interactions and long electron mean free paths. These data provide clear evidence of a significant proximity effect in $\text{MgB}_2/\text{M}(20)$ composite wires with high λ^* metal additions.

Figure 10. Magnetic field dependent transport properties of $\text{MgB}_2/\text{Ga}(20)$ PIT wire at 4.2K. (a) The critical current density (J_c) and critical current (I_c) as determined using the 1 $\mu\text{V}/\text{cm}$ electric field criterion. (b) The n -value as determined from the electric field versus current data. The applied magnetic field was oriented parallel to the wire axis for all measurements.

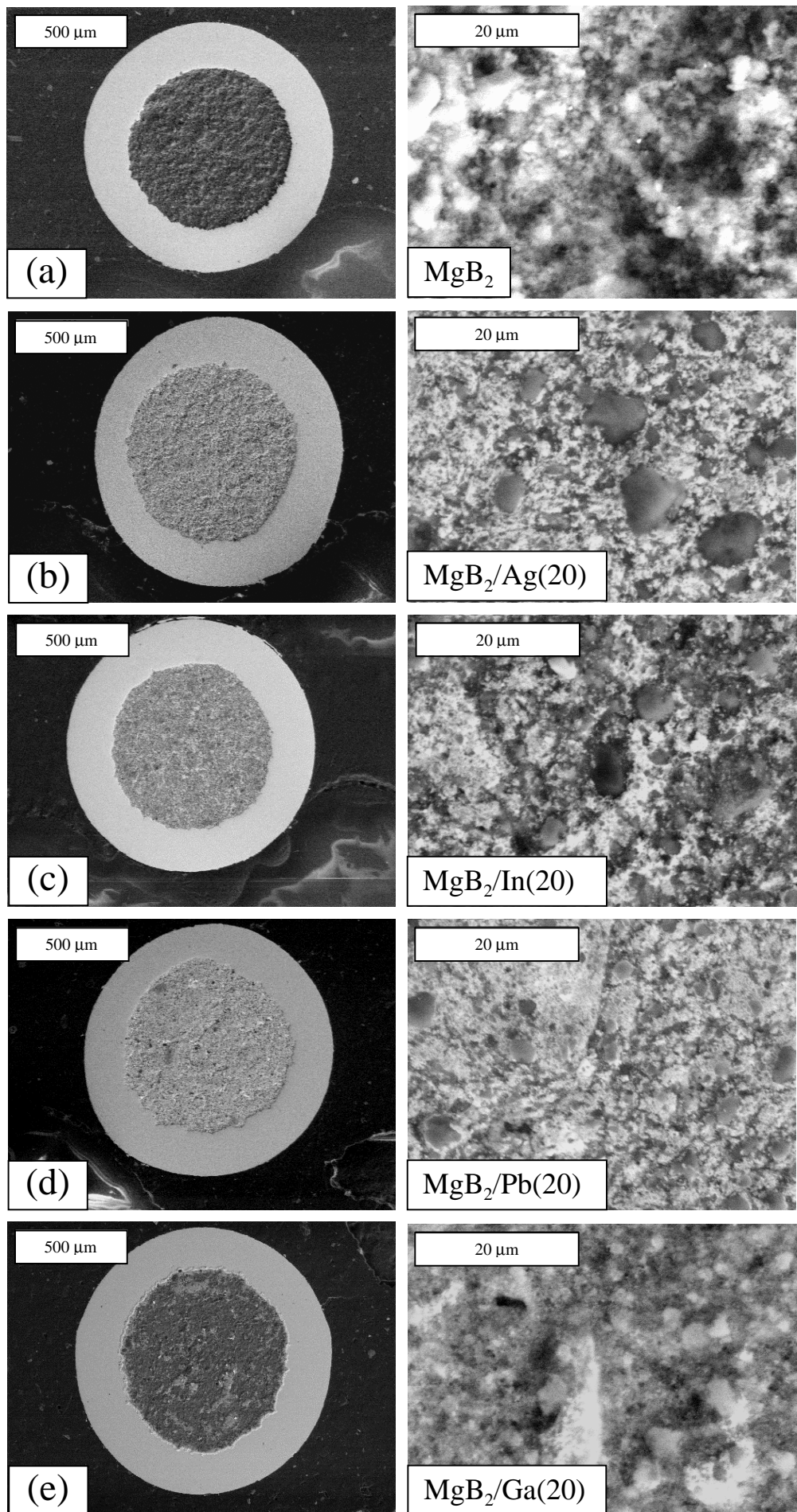


Figure 1.
Holcomb

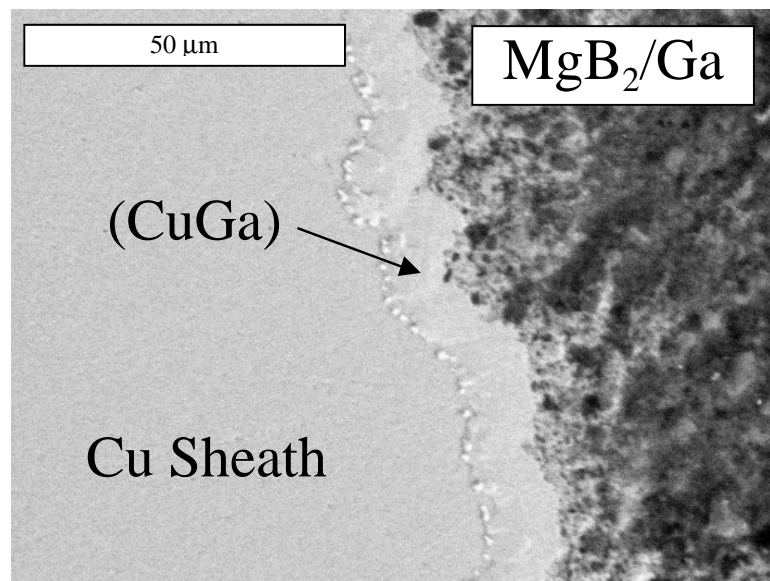


Figure 2. Holcomb

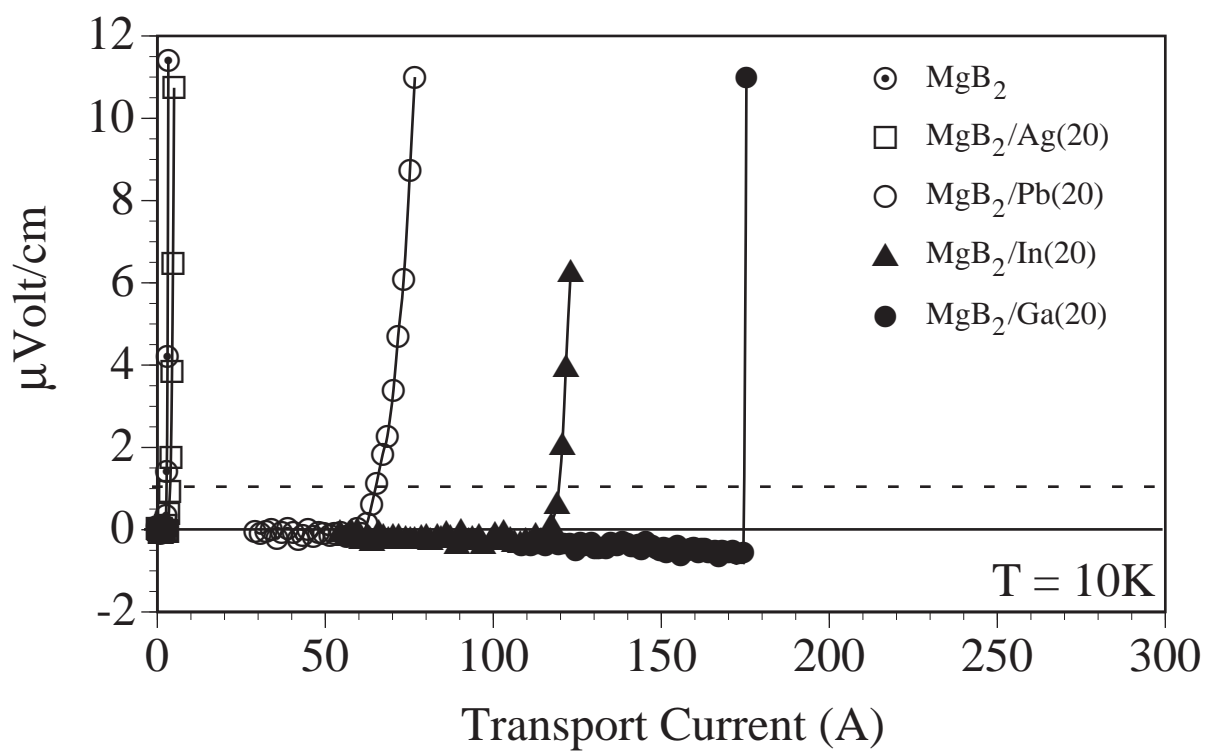


Figure 3. Holcomb

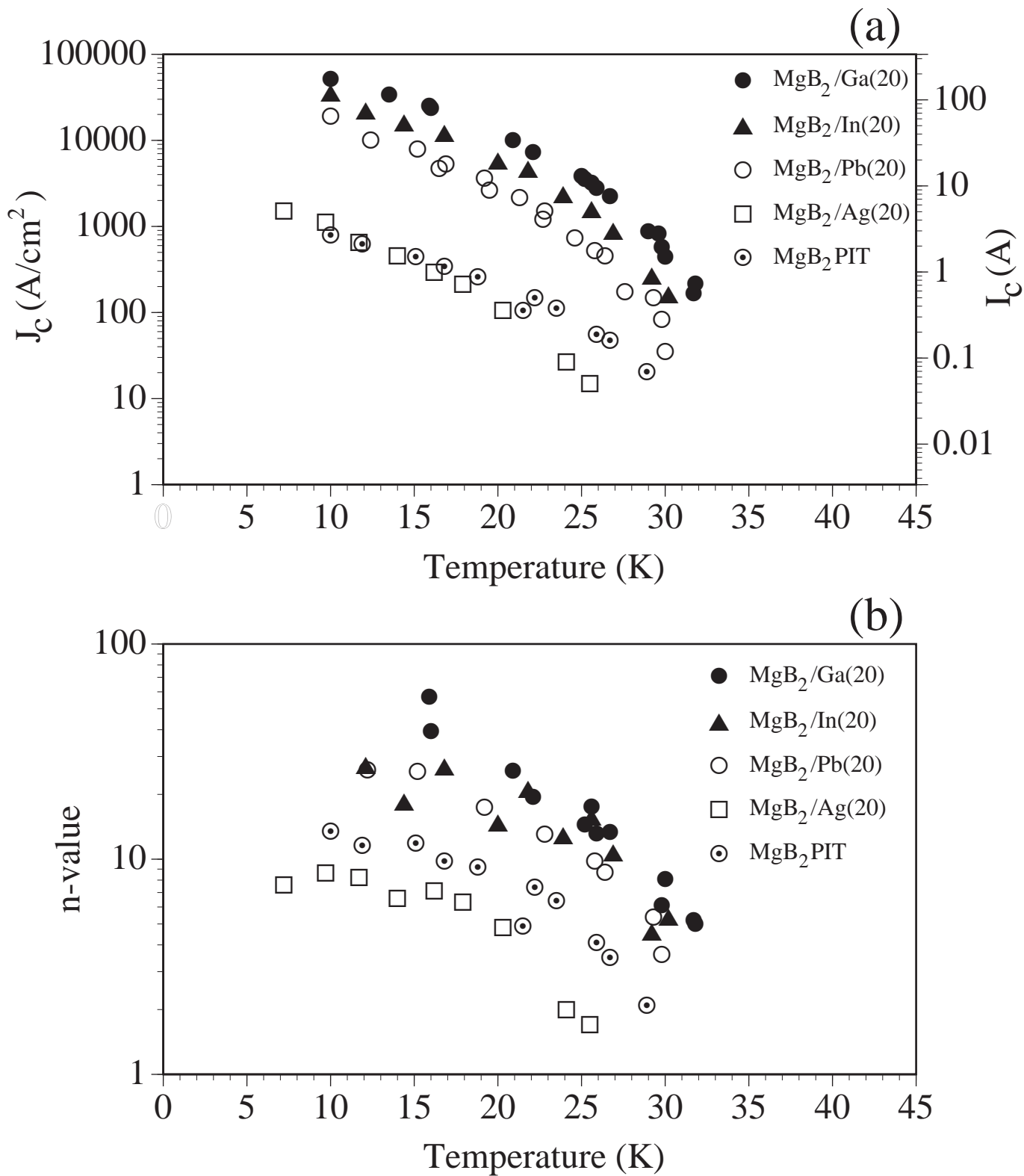


Figure 4. Holcomb

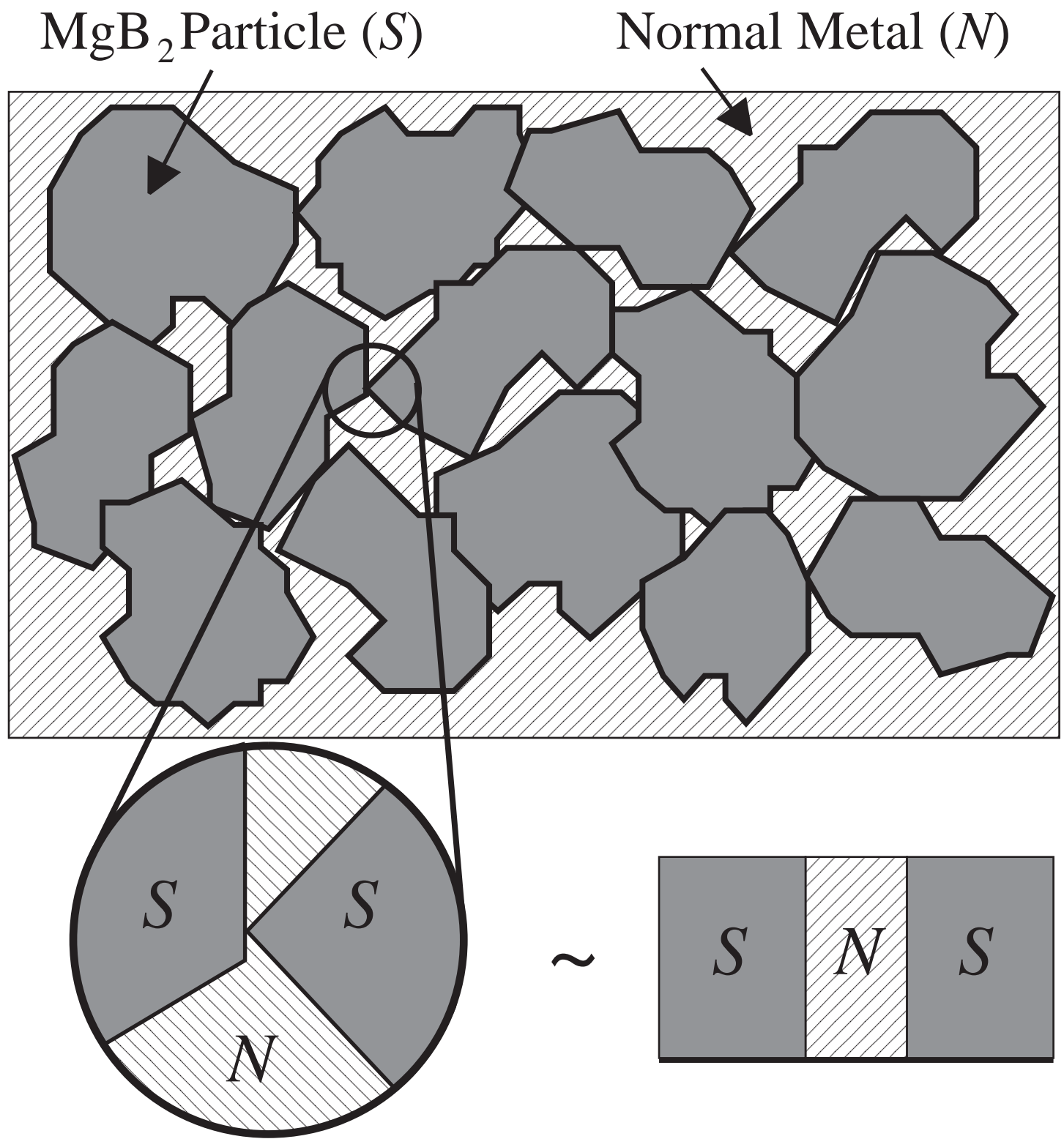


Figure 5. Holcomb

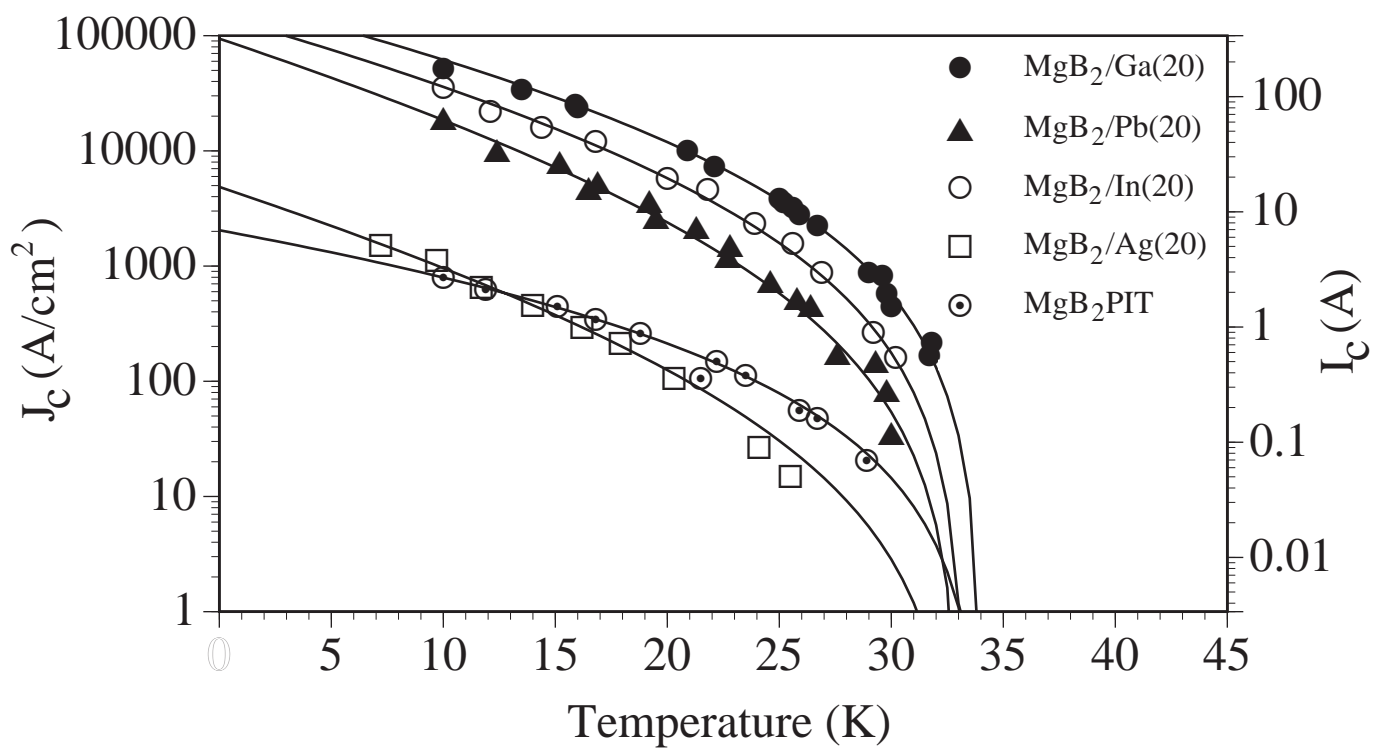


Figure 6. Holcomb

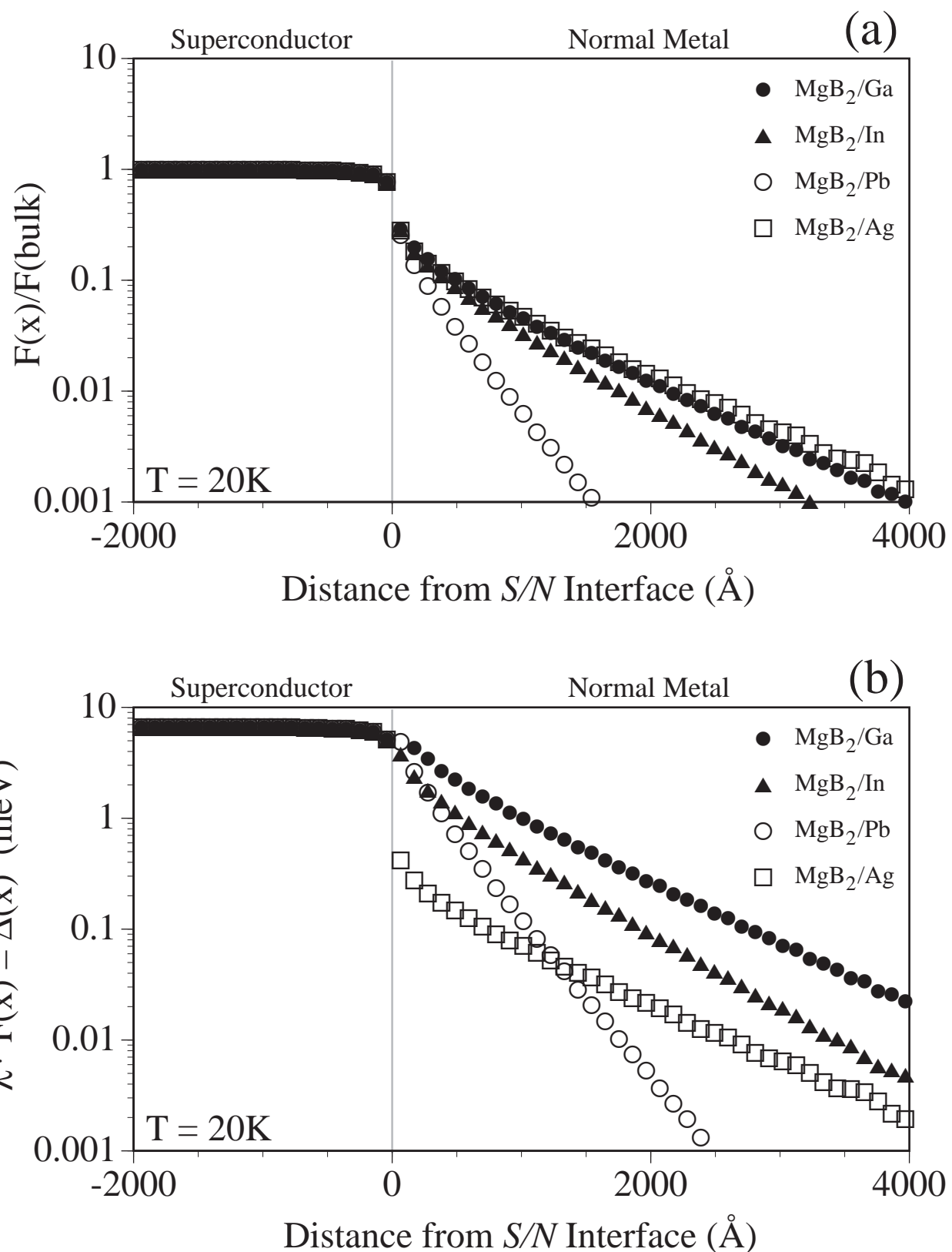


Figure 7. Holcomb

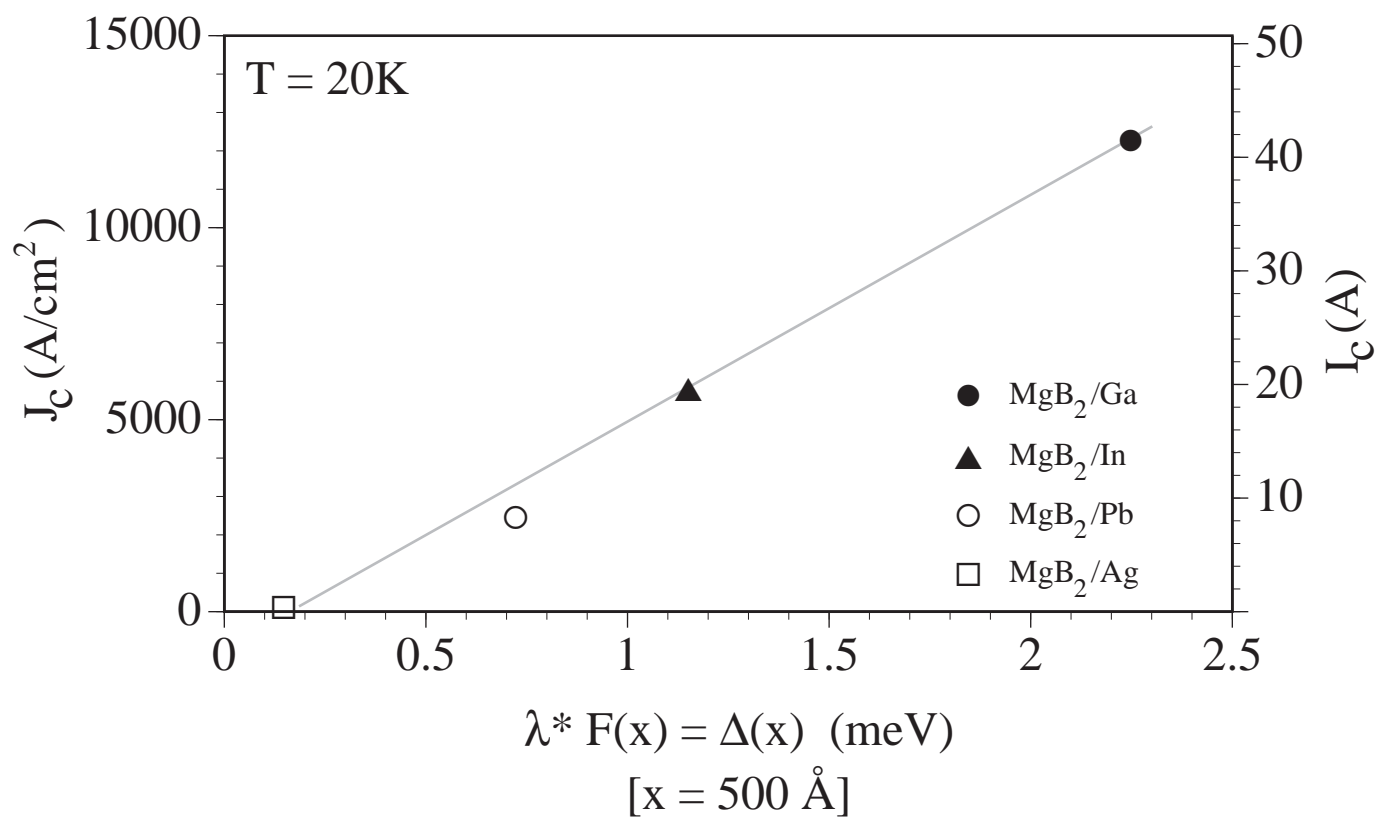


Figure 8. Holcomb

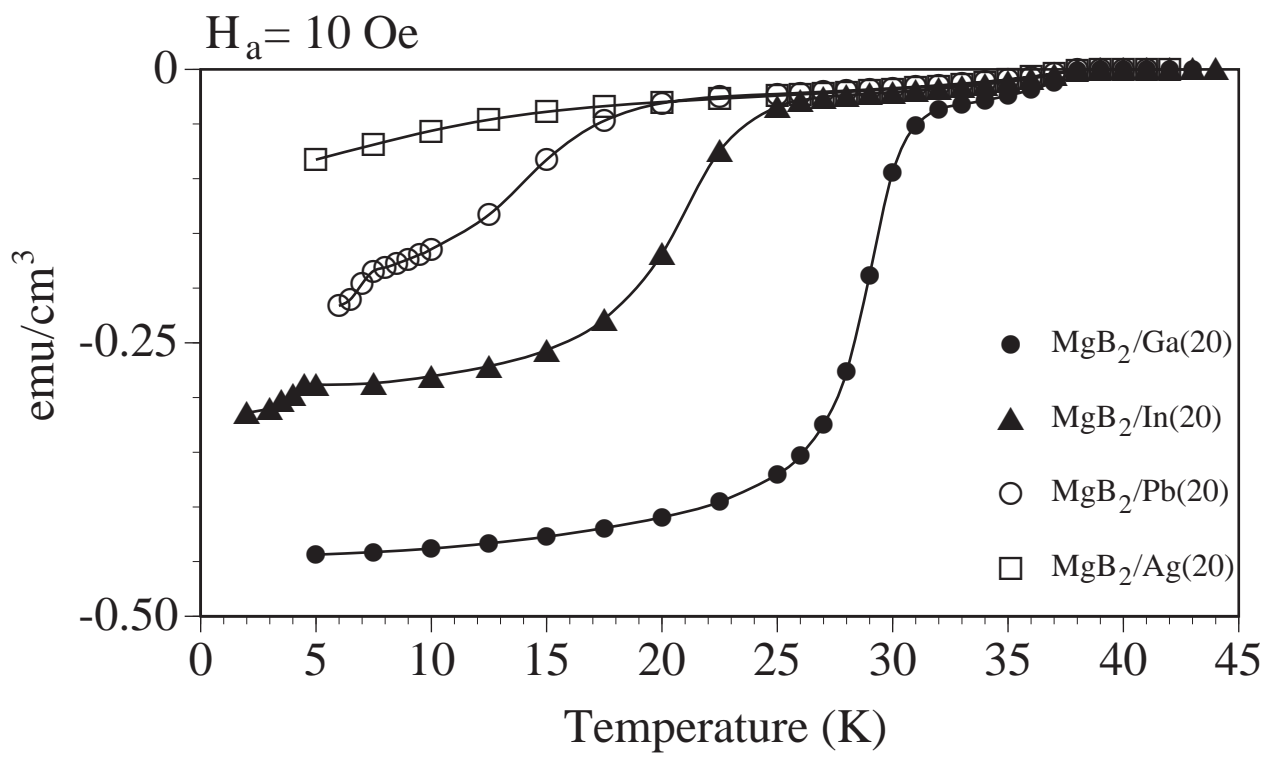


Figure 9. Holcomb

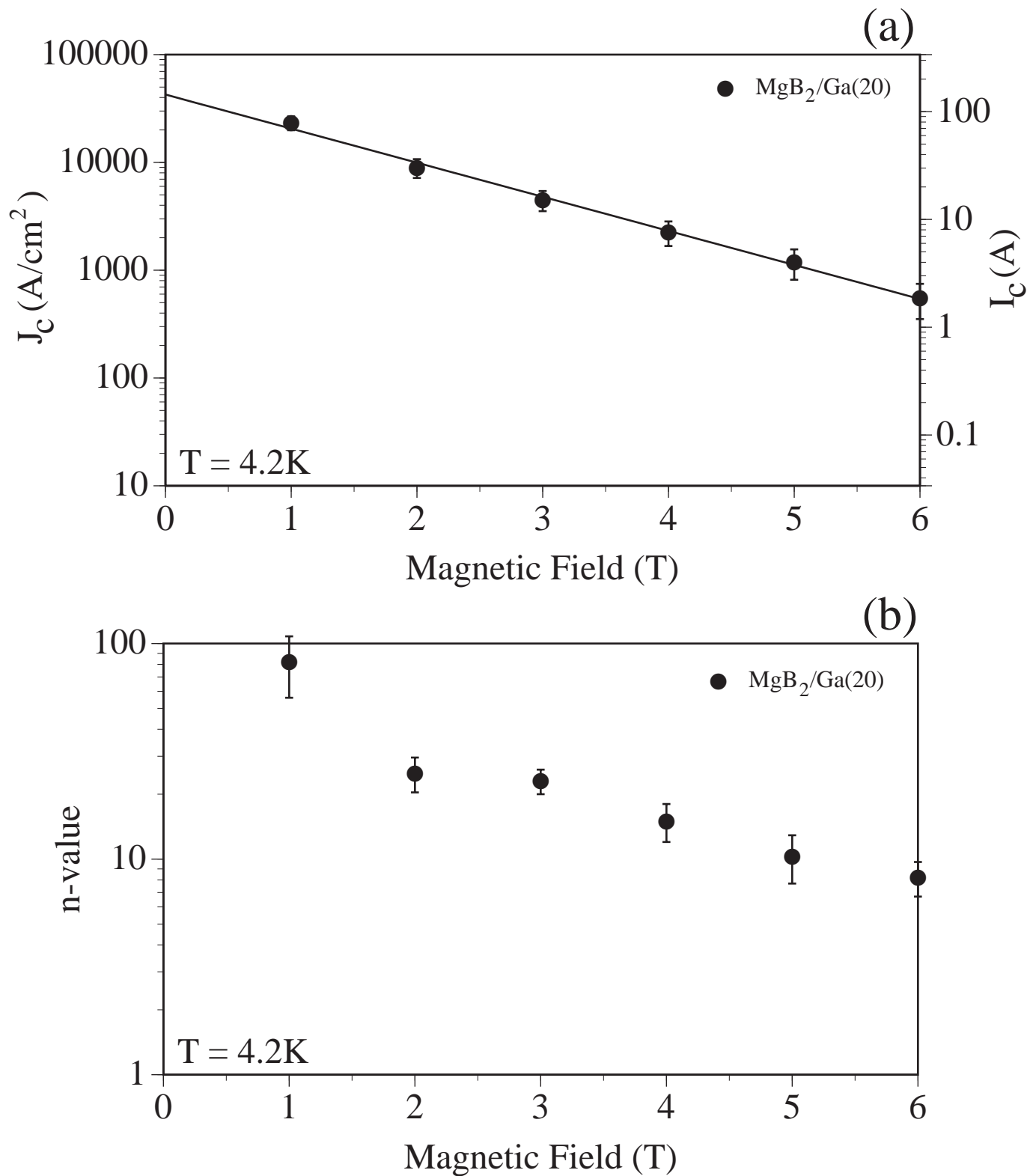


Figure 10. Holcomb

Sample	I_c (A)	J_c (kA/cm ²)	n-value
MgB_2	2.7	0.85	14
$MgB_2/Ag(20)$	3.8	1.11	9
$MgB_2/Pb(20)$	65	18.2	14
$MgB_2/In(20)$	119	36.4	53
$MgB_2/Ga(20)$	175	52.3	--

Table I. Critical current, critical current densities and n-values of MgB_2 and $MgB_2/M(20)$ wires at 10K in self-field.

Sample	J_0 (kA/cm ²)	d (Å)	T_c (K)	v_F (10 ⁸ cm/s)	K_N^{-1} (Å) at 20K	$\text{Exp}(-K_N^{-1}d)$ at 20K	$(1-T/T_c)^2$ at 20K
MgB ₂ /Ag(20)	4.9±0.1	1566±50	33.1±1.1	1.39	845	0.157	0.156
MgB ₂ /Pb(20)	94.6±13.4	2043±270	33.1±0.8	1.83	1112	0.159	0.156
MgB ₂ /In(20)	147.0±4.6	1507±42	33.3±0.5	1.74	1058	0.241	0.160
MgB ₂ /Ga(20)	219.0±14.7	1336±125	34.1±0.4	1.92	1167	0.318	0.171
MgB ₂ PIT	2.0±0.1	274±100	34.2±1.5	0.89	541	0.603	0.172

Table II. Parameters used in the fit of the experimental J_c data.

Material	$v_F (10^8 \text{ cm/s})$	$\rho (\mu\Omega \text{ cm})$ at 20K	$l (\text{\AA})$ at 20K	λ	μ^*	λ^*	$K_N^{-1} (\text{\AA})$ at 20K
Ag	1.39	0.034	24,679	0.15	0.1	0.04	845
Pb	1.83	0.56	869	1.55	0.144	0.55	1112
In	1.74	0.16	3340	0.81	0.116	0.38	1058
Ga	1.92	0.09	4903	2.25	0.174	0.64	1167

Table III. Parameters Used in the Calculation of $\Delta(x)$ in MgB_2/M Junctions.